

## Joining of stainless-steel specimens with nanostructured Al/Ni foils

J. Wang, E. Besnoin, A. Duckham, S. J. Spey, M. E. Reiss, O. M. Knio, and T. P. Weihs

Citation: *Journal of Applied Physics* **95**, 248 (2004); doi: 10.1063/1.1629390

View online: <https://doi.org/10.1063/1.1629390>

View Table of Contents: <http://aip.scitation.org/toc/jap/95/1>

Published by the [American Institute of Physics](#)

---

### Articles you may be interested in

#### [Room-temperature soldering with nanostructured foils](#)

*Applied Physics Letters* **83**, 3987 (2003); 10.1063/1.1623943

#### [Reactive nanostructured foil used as a heat source for joining titanium](#)

*Journal of Applied Physics* **96**, 2336 (2004); 10.1063/1.1769097

#### [Effect of reactant and product melting on self-propagating reactions in multilayer foils](#)

*Journal of Applied Physics* **92**, 5474 (2002); 10.1063/1.1509840

#### [Protein labeling reactions in electrochemical microchannel flow: Numerical simulation and uncertainty propagation](#)

*Physics of Fluids* **15**, 2238 (2003); 10.1063/1.1582857

#### [Characteristics of coherent vortical structures in turbulent flows over progressive surface waves](#)

*Physics of Fluids* **21**, 125106 (2009); 10.1063/1.3275851

#### [Investigation of coupled air-water turbulent boundary layers using direct numerical simulations](#)

*Physics of Fluids* **21**, 062108 (2009); 10.1063/1.3156013

---



# Instruments for Advanced Science

Contact Hiden Analytical for further details:  
W [www.HidenAnalytical.com](http://www.HidenAnalytical.com)  
E [info@hiden.co.uk](mailto:info@hiden.co.uk)

[CLICK TO VIEW](#) our product catalogue




#### Gas Analysis

- dynamic measurement of reaction gas streams
- catalysis and thermal analysis
- molecular beam studies
- dissolved species probes
- fermentation, environmental and ecological studies




#### Surface Science

- UHV TPD
- SIMS
- end point detection in ion beam etch
- elemental imaging - surface mapping



#### Plasma Diagnostics

- plasma source characterization
- etch and deposition process reaction kinetic studies
- analysis of neutral and radical species



#### Vacuum Analysis

- partial pressure measurement and control of process gases
- reactive sputter process control
- vacuum diagnostics
- vacuum coating process monitoring

# Joining of stainless-steel specimens with nanostructured Al/Ni foils

J. Wang<sup>a)</sup>

*Department of Materials Science and Engineering, The Johns Hopkins University, Baltimore, Maryland 21218*

E. Besnoin

*Department of Mechanical Engineering, The Johns Hopkins University, Baltimore, Maryland 21218*

A. Duckham, S. J. Spey, and M. E. Reiss

*Department of Materials Science and Engineering, The Johns Hopkins University, Baltimore, Maryland 21218*

O. M. Knio

*Department of Mechanical Engineering, The Johns Hopkins University, Baltimore, Maryland 21218*

T. P. Weihs

*Department of Materials Science and Engineering, The Johns Hopkins University, Baltimore, Maryland 21218*

(Received 28 July 2003; accepted 6 October 2003)

We describe the joining of stainless-steel specimens at room temperature using free-standing Al/Ni foils as local heat sources for melting AuSn solder layers. The foils contain many nanoscale layers of Al and Ni that react exothermically, generating a self-propagating reaction. The heats, velocities, and products of the reactions are described, and the microstructure and the mechanical properties of the resulting joints are characterized. Increasing the foil thickness, and thereby increasing the total heat released, can improve the strength of the joints until foil thickness reaches 40  $\mu\text{m}$ . For thicker foils, the shear strength is almost constant at 48 MPa, compared to 38 MPa for conventional solder joints. The higher strength is due to finer microstructures in the solder layers of reactive joints. A numerical study of heat transfer during reactive joining and experimental results suggest that the solder layers need to melt completely and remain molten for at least 0.5 ms to form a strong joint. © 2004 American Institute of Physics. [DOI: 10.1063/1.1629390]

## I. INTRODUCTION

Self-propagating exothermic formation reactions have been observed in a variety of nanostructured multilayer foils, such as Al/Ni, Al/Ti, Ni/Si, and Nb/Si foils.<sup>1–7</sup> These reactions are driven by a reduction in atomic bond energy. Once the reactions are initiated by a pulse of energy, such as a small spark or a flame, atomic diffusion occurs normal to the layering as shown schematically in Fig. 1, with A—A and B—B bonds being exchanged for A—B bonds. This bond exchange generates heat very rapidly. Thermal diffusion occurs parallel to the layering and heat is conducted down the foil and facilitates more atomic mixing and compound formation, thereby establishing a self-propagating reaction along the foil. The speeds of these self-propagating exothermic reactions are dependent on layer thickness and can rise as high as 30 m/s,<sup>2,4,8,9</sup> with maximum reaction temperatures above 1200 °C.<sup>9</sup>

Reactive multilayer foils provide a unique opportunity to dramatically improve conventional soldering and brazing technologies by using the foils as local heat sources to melt solder or braze layers and thereby join components, as shown schematically in Fig. 2. This process eliminates the need for furnaces or other external heat sources, and with very localized heating, temperature sensitive components or materials can be joined without thermal damage. Reactive

foil soldering or brazing can be performed at room temperature and in air, argon, or vacuum.

In this work, room-temperature soldering of gold-coated stainless-steel specimens was investigated using free-standing Al/Ni nanostructured multilayer foils and free-standing AuSn solder layers. Thicknesses of the reactive foils were varied in order to optimize the joining of the stainless-steel specimens and to minimize the heating to the specimens. The reaction products of these Al/Ni foils, and the heats and the velocities of the reactions were characterized using x-ray diffraction (XRD), differential scanning calorimetry (DSC), and optical measurements. The measured values were used as inputs to numerically predict thermal transport during the joining process. More specifically, the volume and duration of the melting of the AuSn solder layers and the temperature profiles across the joints were predicted. To validate these predictions, the total time for joining and the temperature rise in the components were measured using infrared imaging. Lastly, the microstructure and mechanical strength of the resulting joints were characterized using scanning electron microscopy (SEM) and tensile shear lap tests, and fracture surfaces were characterized using energy dispersive x-ray (EDX) and optical stereomicroscopy to identify failure mechanisms.

## II. NUMERICAL AND EXPERIMENTAL METHODS

### A. Numerical methods

A numerical study was performed to predict the amount of AuSn solder layer that melts as the foil thickness is varied.

<sup>a)</sup>Electronic mail: jwang@jhu.edu

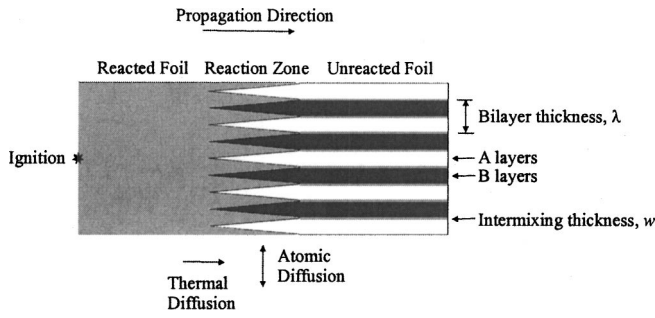


FIG. 1. Schematic drawing of a self-propagating reaction in a multilayer foil, showing a cross-sectional view of the atomic and thermal diffusion that enable reaction formation.  $\lambda$  is the bilayer thickness and  $w$  is the intermixing thickness.

Properties of the foil and components, such as thermal conductivity, heat capacity, heat and velocity of reaction, and foil thickness were incorporated into this model, along with the thermal resistance of the unbonded interface. With all the appropriate inputs, the numerical model was then used to predict the duration of the melting of the AuSn solder at the interface between the AuSn solder and the stainless-steel components, as well as temperatures within the stainless-steel components during bonding.

The model is based on a simplified description of self-propagating reactions that relates the nanoscale transport and kinetic phenomena within the foil, which govern the self-propagation, with the thermal transport and phase evolution, which occur in the AuSn solder layers and the stainless-steel components. The model assumes one-dimensional motion of the reaction front, which is described using the experimentally determined heats and velocities of the reactions. The model also assumes that the joining geometry is such that the effects of convective phenomena in the molten solder layers are negligible. Similarly, the potential pressure-driven flow within the molten solder is not considered. Our computation focuses on simulating heat flow into the solder layers, phase changes within these layers, and temperature evolution within the bonded components. The temperature evolution can be obtained by integrating the energy conservation equa-

tion, which is independently solved within the reactive foil, solder layers, and stainless-steel components:

$$\rho \frac{\partial h}{\partial t} = \nabla \cdot q + \dot{Q}, \quad (1)$$

where  $\rho$  and  $h$  are the density and enthalpy of the corresponding layer,  $t$  is time,  $q$  is the heat flux vector, and  $\dot{Q}$  is the heat release rate. The enthalpy,  $h$ , is related to the temperature,  $T$ , through a relationship that involves the heat capacity,  $c_p$ , and the latent heat,  $h_f$ , of the material. The term  $\dot{Q}$  represents the rate of heat released by the self-propagating front as it traverses the reactive foil. Note that  $\dot{Q}$  is localized within the front that traverses the foil, and vanishes within the fusible material(s) and the components. A third-order finite-difference discretization of the energy equations is used in conjunction with explicit third-order time integration of the discretized evolution equations. The boundary conditions for the temperature in each layer are determined using a thermal interface model. The model accounts for thermal resistance effects at the physical interfaces between unbonded layers and assumes that the thermal resistance exponentially decreases when melting and wetting occur at the interface. In addition, a simplified lumped parameter model was developed for the layers which are significantly thinner than the characteristic thermal thickness of the corresponding material. The temperature across such layers can be treated uniformly and described using the “section-averaged” quasi-one-dimensional conduction equation

$$\frac{\partial T_l}{\partial t} = k_l \frac{\partial^2 T_l}{\partial y^2} + \frac{k_{(l+1)}}{\delta_p} \frac{\partial T}{\partial x} \Big|_{l+1} - \frac{k_{(l-1)}}{\delta_p} \frac{\partial T}{\partial x} \Big|_{l-1}, \quad (2)$$

which involves the heat flux from the adjacent layers ( $l - 1$ ) and ( $l + 1$ ) into the lumped layer ( $l$ ).  $\delta_p$  is the “nominal” layer thickness,  $k_l$  is the thermal conductivity of the layer ( $l$ ), and  $T_l$  is the temperature of the layer ( $l$ ). This asymptotic model is used to compute the temperature evolution in thin coating layers (Au and Incusil) and proves particularly useful for computations that extend over hundreds of milliseconds. The validity of this approach was confirmed by comparing the results obtained with the full model to results from the lumped parameter model.

### B. Experimental methods

Reactive multilayer Al/Ni foils of different thickness were fabricated by magnetron sputtering from Al (Al–0.7 wt % (Si, Fe)–0.1 wt % Cu) and Ni (Ni–7 wt % V) targets onto cooled brass substrates that were rotated in front of the targets. The deposition rates from these targets were chosen so that the relative Al and Ni layer thicknesses were maintained at a 3 to 2 ratio to obtain foils with an overall composition ratio of one Al to one Ni. There were two separate sputtering runs. In both runs, the bilayer thicknesses ranged from 25 to 90 nm. For the first run, the foils contained 640 Al and Ni bilayers and the total foil thicknesses of these foils ranged from 16  $\mu\text{m}$  to 58  $\mu\text{m}$ . For the second run, the foils contained 2000 Al and Ni bilayers and the total thicknesses of these foils ranged from 50 to 180  $\mu\text{m}$ . The base pressure

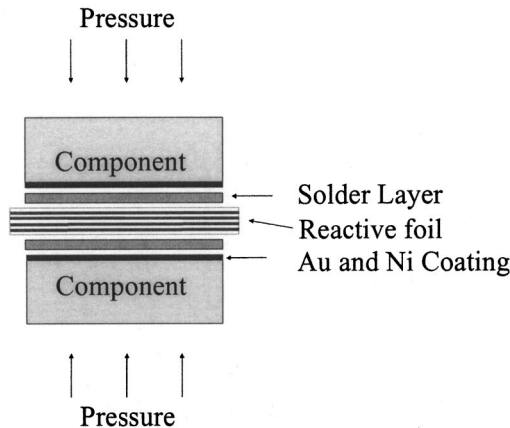


FIG. 2. Schematic showing the reactive joining of two components using a reactive multilayer foil, two solder layers, and an applied pressure.

of the chamber prior to deposition was less than  $1 \times 10^{-6}$  Torr and the pressure of the ultrahigh-purity Ar during deposition was 1 mTorr. To enhance wetting of the foils by the AuSn solder during joining, the foils were coated with a 1  $\mu\text{m}$  thick wetting layer of braze (59 wt % Ag–27.25 wt % Cu–12.5 wt % In–1.25 wt % Ti, Incusil ABA, Wesgo Metals). The braze was deposited under 5 mTorr of Ar, both before and after the Al/Ni multilayer was deposited. Afterwards, the reactive multilayer foils were removed from the brass substrates for use as free-standing foils.

The heat released when an Al/Ni foil is ignited is termed the heat of reaction, and was measured for these foils using a Perkin–Elmer differential scanning calorimeter.<sup>10</sup> In each DSC run, 7–10 mg of free-standing foil were heated from 50 °C to 725 °C at a rate of 40 °C/min in flowing Ar. A baseline was obtained by repeating the heating cycle, which was then subtracted from the heat flow in the first run. By integrating the net heat flow with respect to time, the heat of reaction was obtained.<sup>11,12</sup>

Reaction velocities were measured using a series of optical fibers that have a known periodic spacing as described earlier.<sup>13</sup> As the reactions propagate in front of the fibers, the fibers are illuminated sequentially and the total absorbed light is coupled and sent to one photodiode which is connected to an oscilloscope. Using the resulting voltage signal and the spacing of the optical fibers, reaction velocities can be determined. To characterize the reaction products, free-standing Al/Ni foils were ignited in air and then were ground into powders for symmetric XRD examination using Cu  $K\alpha$  radiation. As-deposited free-standing Al/Ni foils were also examined by XRD for comparison.

Stainless-steel joints were fabricated by stacking two sheets of AuSn solder (80 wt % Au–20 wt % Sn, Williams Advanced Materials) and one reactive foil between two stainless-steel samples, as shown schematically in Fig. 2. The dimensions of the stainless-steel specimens are 0.5 mm  $\times$  6 mm  $\times$  25 mm and were electroplated with Ni and then Au to enhance bonding. The Ni layer serves to promote adhesion to the stainless steel after removal of the native oxide, and the Au coating is designed to prevent surface oxidation and thereby enhance wetting by molten AuSn solder. These stainless-steel samples were joined at room temperature in air by igniting the reactive foils under a pressure of approximately 100 MPa. The joint area was approximately 5 mm by 6 mm. The thicknesses of the reactive Al/Ni foils used here ranged from 20 to 180  $\mu\text{m}$ . After reactive joining, these stainless-steel joints were tested in tension at room temperature using an Instron testing machine and a crosshead speed of 0.1 mm/min. Shear strengths of these joints were obtained by dividing the maximum failure load by the joint area.

For comparison, some stainless-steel specimens were joined using a furnace to heat the AuSn solder instead of a reactive foil. In this case, two stainless-steel specimens and one piece of AuSn solder (25  $\mu\text{m}$  thick) were clamped together and heated in air above the melting temperature of the AuSn solder. Afterward, these conventional stainless-steel joints were tested in tension under the same conditions noted above.

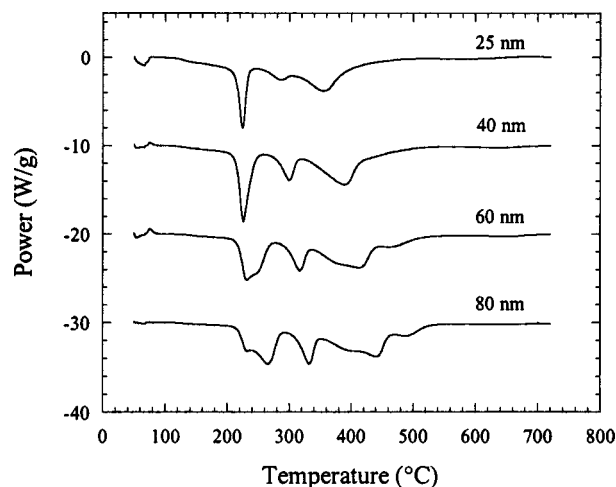


FIG. 3. DSC curves of Al/Ni multilayer foils with different bilayer thicknesses, measured at a heating rate of 40 °C/min.

Cross sections of untested stainless-steel joints were polished to a 1  $\mu\text{m}$  finish and then characterized using a JEOL 6700F scanning electron microscope. In order to understand the failure mechanism of these joints, fracture surfaces of the tested stainless-steel joints were observed using an Olympus SZX12 stereomicroscope and chemical analysis of the fracture surfaces of the joints was performed using EDX analysis.

Temperatures in the stainless steel components were measured during the reaction using an FLIR SC500 infrared camera. Before joining, the sides of the stainless steel specimens were carefully polished to a 6  $\mu\text{m}$  finish and painted white, to ensure a uniform emissivity. Then the temperatures at the side surfaces of the components were monitored during the reactive joining using the infrared camera with a spatial resolution of 108  $\mu\text{m}$  and a temporal resolution of 0.2 seconds. Based on a series of thermal profiles, starting prior to ignition, the heating and cooling rates of reactive joining were quantified.

### III. NUMERICAL AND EXPERIMENTAL RESULTS

#### A. Characterization of reactive foils

DSC curves for the Al/Ni multilayer foils with different bilayer thickness are shown in Fig. 3. For the foils with a 25 nm bilayer thickness, three exothermic peaks were observed and the shoulder to the first exotherm begins at 100 °C. For foils with thicker bilayers, small shoulders were observed and the peak temperatures increased with bilayer thickness, as expected.<sup>12</sup> By integrating the heat flows with respect to time, the heat of reaction,  $\Delta H$ , was obtained for each bilayer thickness and the results are plotted versus the bilayer thickness in Fig. 4. The heat of reaction decreases as the bilayer thickness decreases. For the foils with 80 nm bilayer thickness, the heat of reaction is 1200 J/g. While for the thinnest bilayer samples (25 nm), the heat of reaction decreases to 1016 J/g. This indicates that the volume percentage of intermixing between layers, which occurred during the deposition, is significant and leads to heat losses and, consequently, a reduction in the measured heats of reaction.<sup>12</sup> Assuming



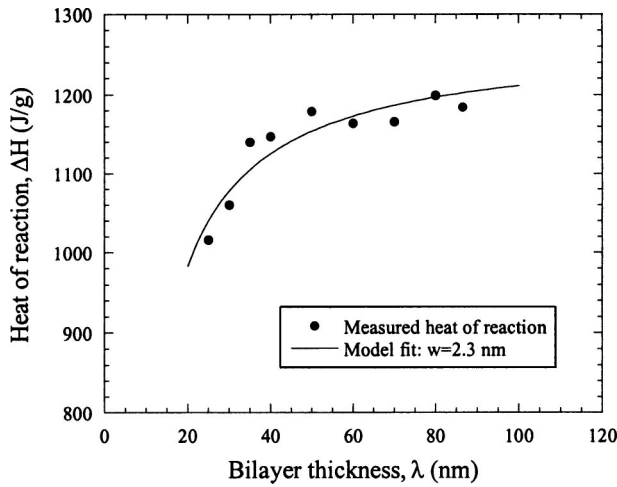


FIG. 4. Heats of reaction as a function of bilayer thickness for Al/Ni reactive foils measured using DSC scans. The curve shown in this plot is fit to the data using Eq. (3),  $\Delta H_0 = 1268$  J/g and  $w = 2.3$  nm.

there is a fixed thickness of atomic intermixing at the Al/Ni interfaces during deposition, heat losses can be assumed to be proportional to  $w/\lambda$  where  $w$  is the intermixing thickness and  $\lambda$  is the bilayer thickness. The heat of reaction can be expressed as

$$\Delta H = \Delta H_0 \left( 1 - \frac{2w}{\lambda} \right), \quad (3)$$

where  $\Delta H_0$  is the enthalpy of formation for the compound that is produced. The measured heats of reaction are plotted versus  $1/\lambda$  in Fig. 5 and a linear line was fit to the data set.  $\Delta H_0$  can be quantified using the intercept at  $1/\lambda = 0$ , which represents a foil with macroscopic layers and nanoscale intermixing,  $w$ . Similarly, the intermixing thickness,  $w$ , can be determined using Eq. (3) and the slope of the line shown in Fig. 5. We estimated that the intermixing thickness,  $w$ , in these Al/Ni foils is  $2.3 \pm 0.3$  nm and the maximum heat of reaction,  $\Delta H_0$ , is  $1268 \pm 21$  J/g. With these given values of  $\Delta H_0$  and  $w$ , heats of reaction can be calculated for all the

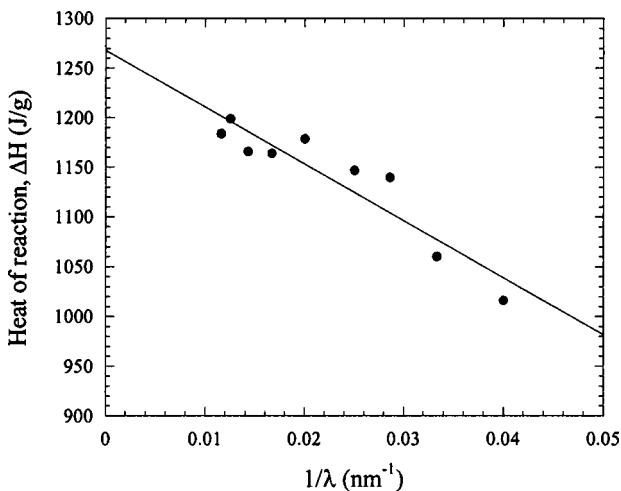


FIG. 5. Heats of reaction as a function of  $1/\lambda$ . Maximum heat of reaction,  $\Delta H_0$ , and intermixing thickness,  $w$ , were determined to be  $1268 \pm 21$  J/g and  $2.3 \pm 0.3$  nm, respectively.

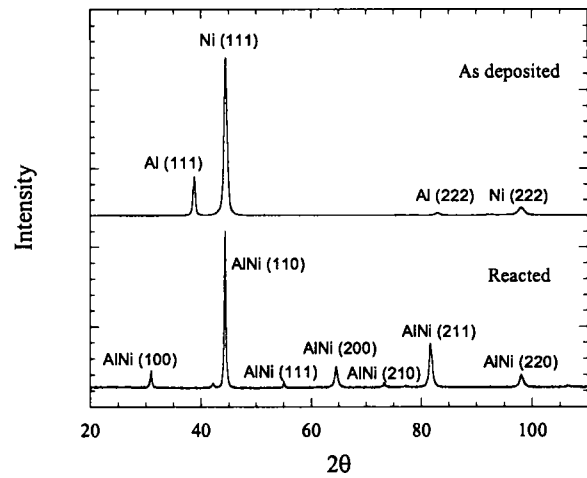


FIG. 6. XRD patterns for Al/Ni multilayer foils before and after a reaction. The peaks in the scan for the as-deposited foil correspond to textured Ni and Al. The major peaks in the scan for the reacted foil correspond to the ordered B2 AlNi compound. One unidentified peak might be related to the  $Al_6V$  compound.

bilayer thicknesses and are plotted in Fig. 4. These calculated heats of reaction were used as inputs for the numerical predictions of thermal transport during the joining process.

Reaction velocities for all samples were measured and were found to increase from 3.5 to 7 m/s, as bilayer thickness decreased from 90 to 25 nm. This inverse dependence of velocity on bilayer thickness suggests that the reaction velocity is mainly determined by the average diffusion distance, and not the heat of reaction and reaction temperature as is seen for very small bilayers.<sup>9,14,15</sup> As bilayer thickness decreases from 90 to 25 nm, the diffusion distances are smaller and atoms can mix more rapidly so heat is released at a higher rate and the reactions travel faster through the foils.

XRD traces for as-deposited and reacted Al/Ni foils are plotted in Fig. 6. Before the reaction, all major peaks correspond to Al and Ni, as shown in the upper scan in Fig. 6. After the reaction, all major peaks correspond to the ordered B2 AlNi compound, which is the equilibrium compound for this composition, as shown in the lower scan in Fig. 6. There is an unidentified peak in the scan which might be related to the  $Al_6V$  compound in the final product. When the foils are reacted during the joining process, the B2 AlNi compound is expected to be the dominant product.

## B. Numerical results

The predictions of the melting of the AuSn solder layers during reactive joining of stainless steel are shown in Fig. 7 as a function of the thickness of the Al/Ni foils. The numerical results show that the amount of AuSn solder that melts increases as the foil thickness rises from 0 to 22  $\mu\text{m}$ . For foils thicker than 22  $\mu\text{m}$ , the whole 25  $\mu\text{m}$  thick AuSn solder layer melts, which is thought to be necessary for bonding. Note also that the predictions show that the duration of the period, during which the whole AuSn solder layer is molten, increases with increasing foil thickness, as shown in Fig. 7.

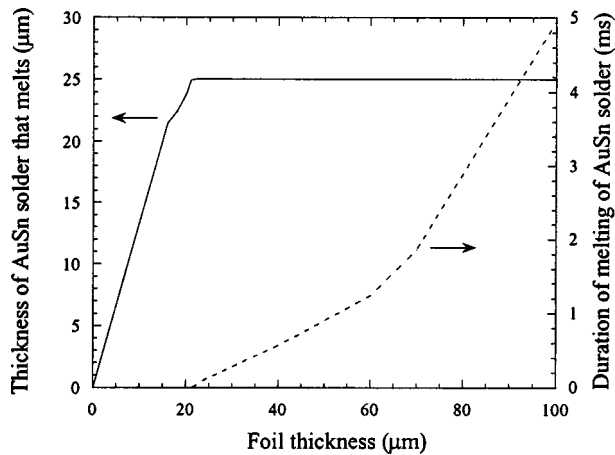


FIG. 7. Numerical predictions of the thickness of AuSn solder that melts and the duration of the melting at the interface between the AuSn solder and the stainless-steel components, as a function of foil thickness.

As the foil thickness increases from 22 to 100  $\mu\text{m}$ , the duration of the melting of the AuSn solder layer rises from 0 to 5 ms.

Temperature profiles across the stainless-steel joint, both during and after the reaction, were predicted numerically and the results are shown in Fig. 8. These curves represent the temperature profiles across the joint at the moment of ignition, and at 0.1 ms, 0.5 ms, 1.0 ms, 10.0 ms, 50.0 ms, and 400.0 ms after the start of the reaction. The results show very localized heating in the components and very rapid cooling across the joint. It is predicted that the maximum temperatures across the joint decreases to 48  $^{\circ}\text{C}$  only 400 ms after ignition.

Figure 9 shows temperature changes in the stainless-steel components 100  $\mu\text{m}$  from the interface with the solder layer. Values were obtained from both numerical predictions and experimental measurements. The numerical results predict that the temperature will decrease to 60  $^{\circ}\text{C}$ , 0.2 s after ignition and that the heat exposure to the stainless-steel com-

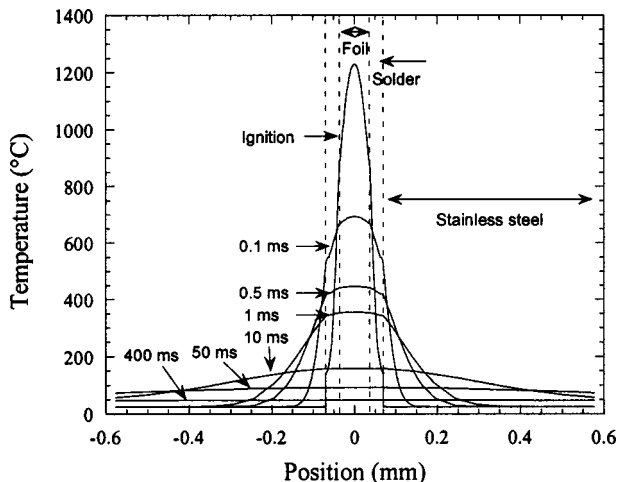


FIG. 8. Temperature profiles across a stainless-steel joint obtained from numerical predictions. The thicknesses of the foil and the solder layers are 70  $\mu\text{m}$  and 25  $\mu\text{m}$ , respectively, and the position 0 is the center of the foil.

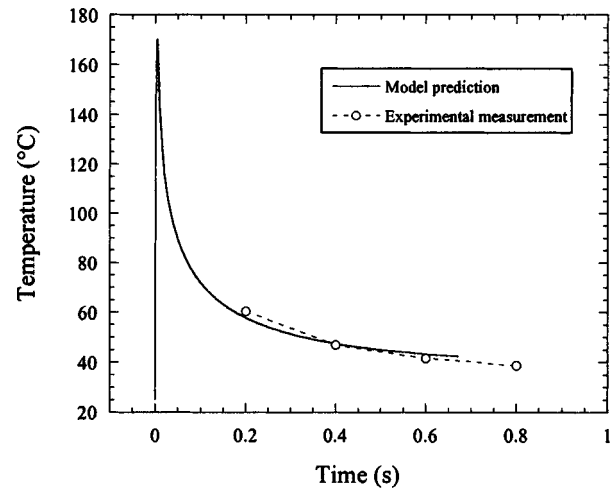


FIG. 9. Temperature changes in a stainless-steel component, 100  $\mu\text{m}$  from the solder/stainless-steel interface, from both numerical predictions and experimental measurements.

ponents is very limited and localized, particularly when compared to traditional soldering methods that utilize furnaces.

### C. Thermal characterizations

Temperatures in the stainless-steel components were measured during the reactive joining process using an infrared camera for the case of a 70  $\mu\text{m}$  Al/Ni foil and two 25  $\mu\text{m}$  thick AuSn solder layers (one on either side of the foil). Based on a series of thermal profiles, it was estimated that the total heating time is less than 0.2 s. After the reaction is completed, temperatures in the stainless-steel specimens decreased very quickly. In the stainless-steel components, 100  $\mu\text{m}$  from the interface with the solder layer, the temperature decreased to 60.4  $^{\circ}\text{C}$  and 38.8  $^{\circ}\text{C}$  at 0.2 s and 0.8 s after ignition, respectively, as shown in Fig. 9. Based on these measurements, the cooling rate is estimated to be  $>1000^{\circ}\text{C/s}$ . This is very consistent with the numerical predictions described earlier. With such rapid heating and cooling of the components, thermal exposure is very limited, particularly when compared to traditional furnace soldering. This is a very useful advantage for joining temperature sensitive materials and components such as specialty alloys and microelectronic devices.

### D. Microstructural and mechanical characterizations

Figure 10(a) shows two stainless-steel specimens that were joined using two pieces of free-standing AuSn solder (25  $\mu\text{m}$  thick) and one Al/Ni reactive foil (80  $\mu\text{m}$  thick). Cracking was observed within the reacted foils and is attributed to the fact that when the foils react they contract due to densification; they also contract due to cooling from the high reaction temperatures. Both sources of contraction can be constrained by the surrounding material, thereby leading to cracking. Molten AuSn solder typically flowed into these cracks, creating a particle composite at the bond interface with hard pieces of reactive foil in a solder matrix. Note that the AuSn solder layers decreased in thickness from 25  $\mu\text{m}$  to several microns, suggesting that the majority of the solder

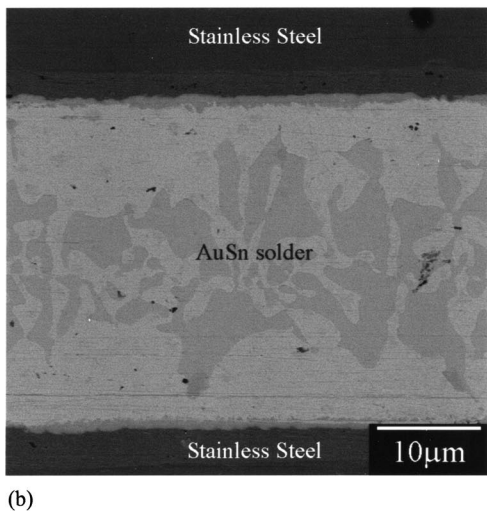
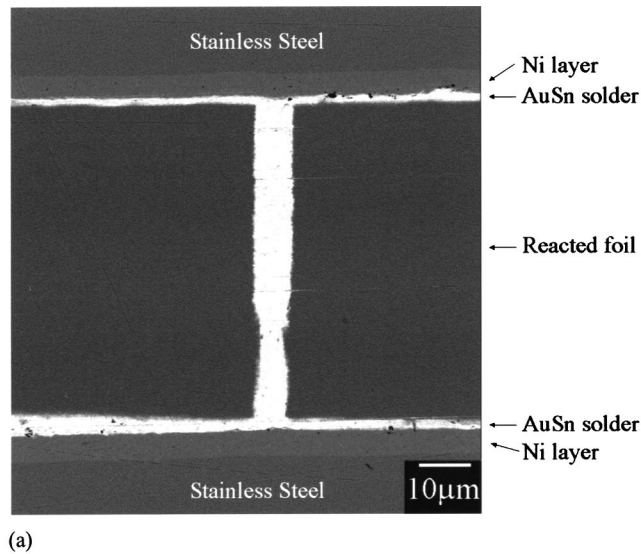


FIG. 10. SEM micrographs of stainless-steel components joined using (a) Al/Ni foils and sheets of free-standing AuSn solder (25  $\mu\text{m}$  thick). Note that most of the Au–Sn solder flows out of the joint and into cracks that form within the foil on reaction and on cooling and (b) conventional furnace soldering. Here, the thickness of the solder layer remains constant at 25  $\mu\text{m}$ , before and after soldering.

flowed into cracks and out of the bond area, due to the applied pressure. Lastly, note that the boundaries between the Au and Ni layers on the stainless-steel samples remain distinct. This suggests that there were insufficient time and temperature along the surfaces of the specimens to enable significant intermixing of the Au and Ni layers. The microstructure of the AuSn solder layer is shown in Fig. 11(a) at a higher magnification. A very fine lamellar eutectic structure is observed in Fig. 11(a), suggesting a light Au-rich phase ( $\xi$  phase,  $\text{Au}_5\text{Sn}$ ) and a dark Sn-rich phase ( $\delta$  phase, AuSn), which are the equilibrium phases for this composition. These two phases grow simultaneously and form parallel plates in grainlike colonies. The spacing between these plates is approximately 50 nm.

Figure 10(b) shows two stainless-steel specimens that were joined using a piece of free-standing AuSn solder (25  $\mu\text{m}$  thick) and a furnace for heating, followed by air cooling. The thickness of the AuSn solder layer remains at 25  $\mu\text{m}$

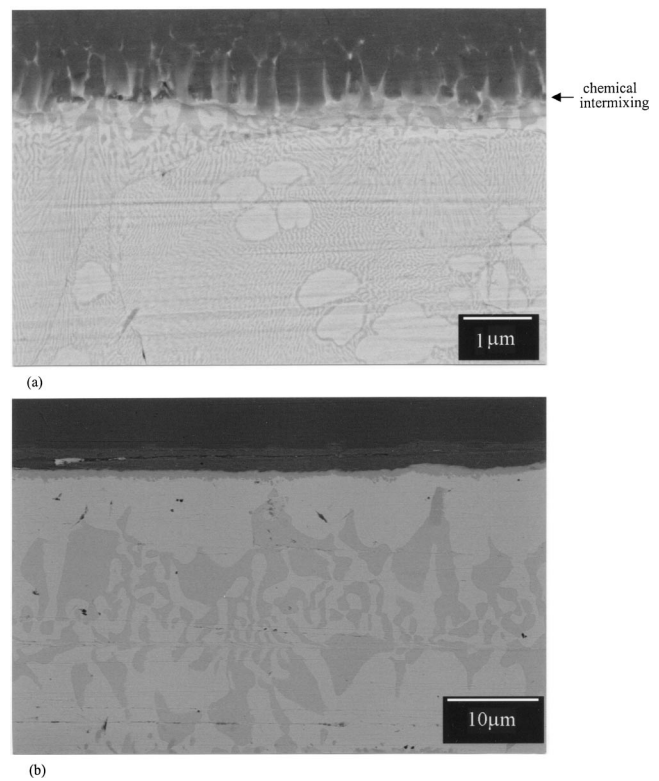


FIG. 11. Microstructures of AuSn solder by (a) reactive joining, showing fine lamellar eutectic structure and chemical intermixing at the Au/AuSn interface, and (b) conventional soldering in furnaces, showing very coarse structure and no chemical intermixing.

after soldering, compared with the several microns thick AuSn layers within the reactive joint. Phase distribution in the solder layer is not uniform. The outer layer solidifies faster than the center of the solder layer and is slightly Au rich. The microstructure of the AuSn solder formed by melting solder in a furnace is much coarser as shown in Fig. 11(b). This is due to the much slower cooling rate in conventional soldering. It contained two phases: A light Au-rich phase ( $\xi$  phase,  $\text{Au}_5\text{Sn}$ ) and a dark Sn-rich phase ( $\delta$  phase, AuSn).

The shear strengths of joints are plotted as a function of foil thickness in Fig. 12. Note that the joint made with the thinnest foil (23  $\mu\text{m}$ ) showed a shear strength of only 2 MPa. Using thicker foils that produce more heat upon reaction yielded significant improvements in shear strength. As the thickness of the foil increases from 23  $\mu\text{m}$  to 40  $\mu\text{m}$ , shear strength rises quickly from 2 MPa to 50 MPa. Further increases in the foil thickness do not affect the shear strength of the stainless-steel joints, which is approximately constant with an average value of  $48 \pm 3$  MPa, for foil thicknesses ranging from 40 to 180  $\mu\text{m}$ .

Optical photographs of fracture surfaces of three reactive foil joints are shown in Fig. 13, identifying trends with foil thickness. When the reactive foil is very thin, e.g., 23  $\mu\text{m}$ , there is little wetting of AuSn solder onto the Au-coated stainless-steel specimens [Fig. 13(a)]. While the wetting is limited, it does suggest that the AuSn solder layer has melted across its full thickness as predicted in Fig. 7. As the thickness of the reactive foil increases, the duration that solder

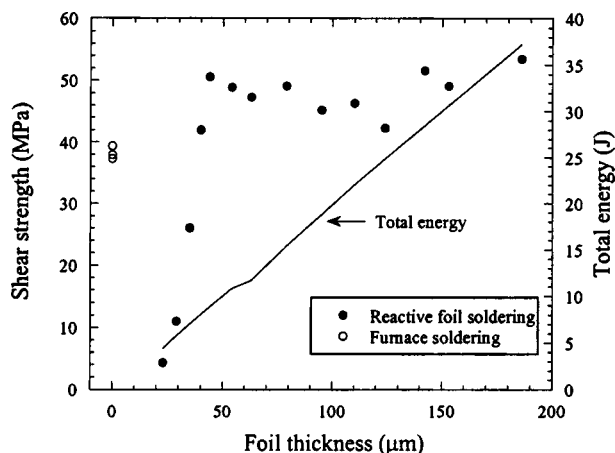


FIG. 12. Shear strength of stainless-steel joints and total energy released from Al/Ni reactive foils as a function of foil thickness. The total energy released from Al/Ni foils is based on Eq. (3) and data shown in Fig. 4.

layers remain molten rises, and there is additional wetting of the specimens by the AuSn solder [Fig. 13(b)]. When the reactive foil is sufficiently thick, there is full wetting of the Au coated stainless-steel specimens as shown in Fig. 13(c), suggesting that, in this case, the duration of the AuSn layer remaining molten is long enough to ensure complete wetting of the Au-coated stainless-steel specimens. EDX analysis of the fracture surfaces of the stainless-steel joints shows that Au and Sn are the dominant elements on both sides of the joints. This indicates that failure occurred within the AuSn solder, rather than the solder/foil interfaces or along the solder/specimen interfaces. The reaction product of Al/Ni foil is a fine grained and hard intermetallic which is expected with the rapid cooling and the formation of the B2 ordered structure. Failure of the reactive joint did not occur within the foil itself.

In comparison to these reactive joints, the average shear strength of the stainless-steel joints made by conventional soldering was only  $38 \pm 1$  MPa, as shown in Fig. 12. The lower strengths of these joints can be attributed to their coarser microstructure [Fig. 11(b)], compared to the fine eutectic microstructure [Fig. 11(a)] for reactive multilayer joints that cool very rapidly. It could also be attributed to their thicker ( $25 \mu\text{m}$ ) AuSn solder layer [Fig. 10(b)], compared to the thinner ( $\sim 3 \mu\text{m}$ ) AuSn solder layers [Fig. 10(a)] in the reactive joints. In order to distinguish the influence of both factors, some stainless-steel joints, made by reactive joining with foils thicker than  $40 \mu\text{m}$ , were annealed at the melting temperature of the AuSn solder for 5 min. It was found that the average shear strength of these annealed joints is 39 MPa, similar to the average shear strength of stainless-steel joints formed by conventional furnace soldering. For these joints, the AuSn solder layers are still only several microns thick but now have coarse microstructures. This demonstrates that the lower strengths of the conventional solder joints can be attributed to their coarser microstructures and not to their thicker solder layers, compared to the reactive solder joints.

#### IV. DISCUSSION

The shear strength data in Fig. 12, and the fracture surfaces in Fig. 13, suggest that the shear strength of the joints is controlled by the melting and wetting of the AuSn solder onto the stainless-steel components. The combination of high shear strengths and good wetting, as shown in the SEM images [Fig. 10(a)], also suggests that in order to form a strong joint between the stainless-steel components, the free-standing solder layers must melt across their complete thickness ( $25 \mu\text{m}$ ) and wet the stainless-steel components. The melting of the AuSn solder layer is dependent on the total heat released from the Al/Ni foils during a reaction. The total heat of a reaction, in turn, is dependent on foil thickness in two ways. First, the heat of a reaction  $\Delta H$  (in J/g) varies with bilayer thickness, as shown in Fig. 4 and, consequently, varies with foil thickness. Second, as shown in Fig. 12, the total heat of a reaction (or total energy) also increases with foil thickness, simply because there is a greater volume of foil to react. Both factors must be considered when predicting heat transport during reactive joining. Note that there is a kink in the total energy line at foil thicknesses ranging between 50 and  $65 \mu\text{m}$ . This is due to the variation of the heat of a reaction (in J/g) of foils with bilayer thickness as shown in Fig. 4, and the shift from one set of foils below the kink (640 bilayers) to another set of foils above the kink (2000 bilayers). In particular, the  $50 \mu\text{m}$  thick foils had a bilayer thickness of 78 nm and heat of reaction of 1200 J/g. While the  $65 \mu\text{m}$  foils had a 33 nm bilayer thickness and a heat of reaction of only 1060 J/g. Hence, a kink appears in the total energy line.

Observation of the fracture surfaces of these joints shows that when the reactive foil is very thin, e.g.,  $23 \mu\text{m}$ , there is little wetting of AuSn solder layers onto the stainless-steel components. Here, the joint failed at the interface between the AuSn solder and the stainless-steel components. While the total heat released from this foil during reaction is enough to melt all the AuSn solder layer, the duration of the melting is insufficient to enable complete wetting of the stainless-steel components. Since there is little wetting of the Au-coated stainless-steel specimens, the shear strength of this joint is very low. The measured value of 2 MPa can be attributed to the very limited wetting area. As the thickness of the reactive foil increases, there is more wetting of the AuSn solder layer onto the stainless-steel components, which is consistent with the fact that thicker foils produce more heat, as shown in Fig. 12. When the reactive foil is thick enough, i.e., thicker than a critical value of  $40 \mu\text{m}$ , all of the AuSn solder layer melts and remains molten for over 0.5 ms and there is full wetting of the AuSn solder onto the stainless-steel components. The predictions shown in Fig. 7, together with the shear strength data in Fig. 12, indicate that the full AuSn solder layer needs to be molten for a minimum period of 0.5 ms to establish a strong joint, near 50 MPa for these stainless-steel specimens.

Knowing the total area of the joint ( $5 \text{ mm} \times 6 \text{ mm}$ ), one can calculate the total heat of reaction needed to form a strong joint. Using the density of the foils, specific heat of reaction, and the critical thickness ( $40 \mu\text{m}$ ) of the foil, the



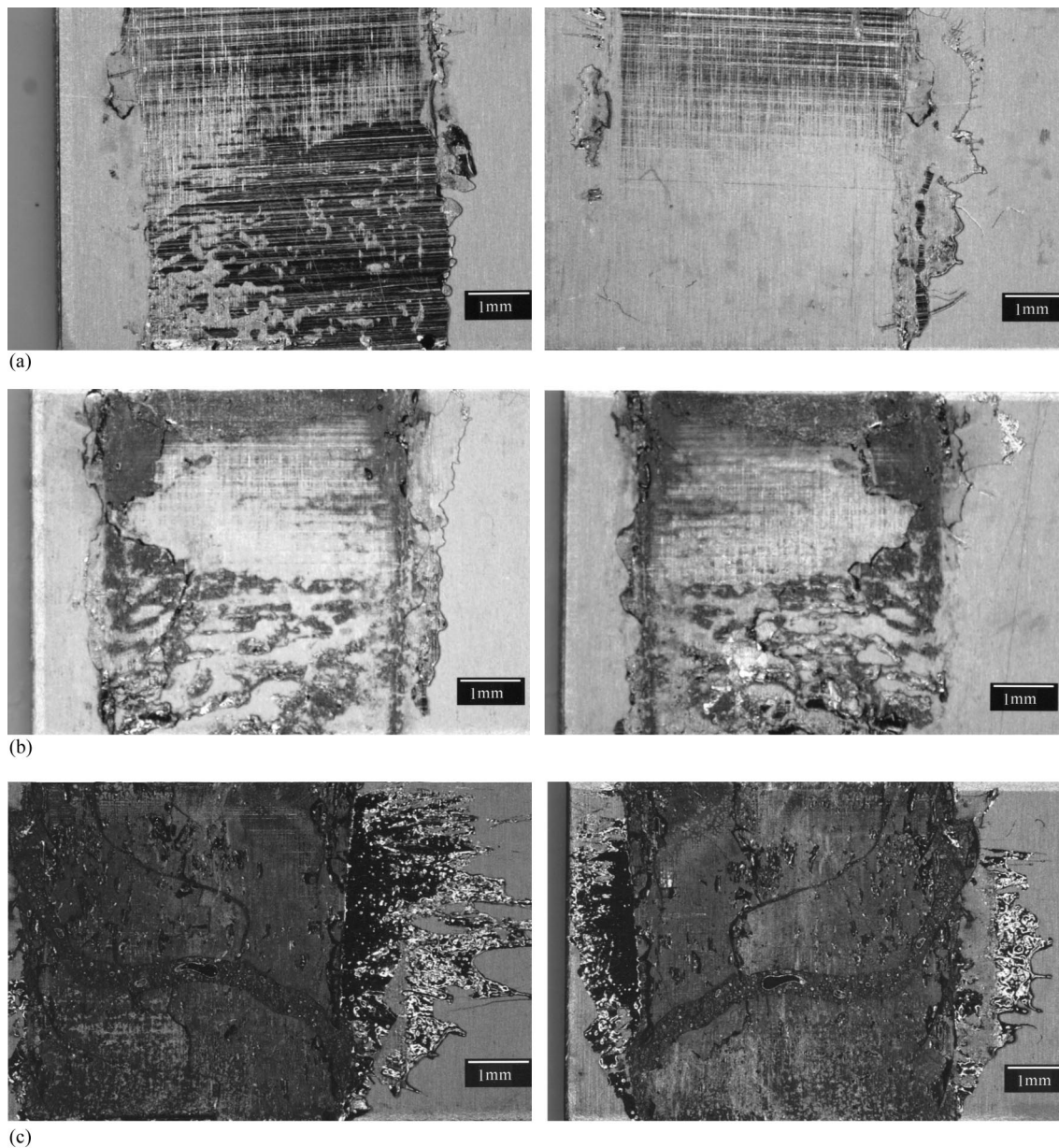


FIG. 13. Fracture surfaces of the stainless-steel joints obtained by optical stereomicroscopy. (a) A joint was formed with a  $23\ \mu\text{m}$  foil and shows little wetting of the Au-coated stainless-steel specimens. (b) A joint was formed with a  $35\ \mu\text{m}$  foil and shows partial wetting of the Au-coated stainless-steel specimens. (c) A joint was formed with a  $79\ \mu\text{m}$  foil and shows full wetting of the Au-coated stainless-steel specimens.

total heat was calculated to be 9 J. This heat is transferred to the AuSn solder layers and stainless-steel components, resulting in the melting of the AuSn solder layers and a strong joint. For comparison, the heat,  $Q$ , needed to melt two AuSn solder layers measuring  $5\ \text{mm} \times 6\ \text{mm} \times 25\ \mu\text{m}$  can be determined by

$$Q = m(T_m - T_{\text{RT}})C_p + m\Delta H_f, \quad (4)$$

where  $m$  is the mass of the two AuSn solder sheets,  $T_m$  is the melting temperature of AuSn solder,  $T_{\text{RT}}$ , room temperature,  $C_p$  is the heat capacity of AuSn solder, and  $\Delta H_f$  is the heat of fusion of AuSn solder (J/g). Using the appropriate density and volume of AuSn solder and Eq. (4),  $Q$  was calculated to be 1.66 J, which is much less than the total critical heat released from the reactive foil, 9 J, as mentioned above. The reason is that by the thermodynamic calculation in Eq. (4),

we only consider the energy required to heat and melt the AuSn solder. This comparison clearly demonstrates that one also needs to consider kinetic heat transport into the solder layers and stainless-steel components to accurately predict the energy required for reactive joining. This is particularly true when one is joining very conductive components such as Al.

Figure 12 also shows that once the foil thickness reaches the critical thickness, i.e.,  $40\ \mu\text{m}$ , further increases in the foil thickness do not improve the shear strength of the stainless-steel joints. The shear strength is effectively constant with an average value of  $48 \pm 3\ \text{MPa}$ , for foil thickness ranging from 40 to  $180\ \mu\text{m}$ . This suggests that when foil thickness is within this range, sufficient heat is released to melt the full solder layer thickness and wet the stainless-steel components

in each joint. Furthermore, it suggests that any additional heat over 9 J does not lead to stronger joints in this particular geometry. Lastly, this also suggests that solder or braze layers with a higher melting temperature could be used in reactive joining with foils thicker than 40  $\mu\text{m}$ .

## V. CONCLUSIONS

In conclusion, we have demonstrated a method of joining Au-coated stainless-steel specimens at room temperature in air using free-standing Al/Ni foils with nanoscale layers and free-standing AuSn solder layers. The reactive foils have heats of reaction up to 1168 J/g, a final product of ordered AlNi, and reaction velocities ranging from 3.5 to 7 m/s, increasing with decreasing bilayer thickness. The self-propagating reactions act as very localized heat sources that melt AuSn solder layers and join the stainless-steel specimens. Using thicker foils increases the available energy and improves the strength of the joints, until a critical thickness of 40  $\mu\text{m}$  is reached. Above 40  $\mu\text{m}$ , the shear strength of the stainless-steel joints is approximately constant at 48 MPa, compared to 38 MPa for conventional solder joints of the same specimens. The higher strengths in the reactive joints are attributed to refined AuSn microstructures that develop on rapid cooling. A comparison of numerical predictions of melting of the AuSn solder layers during reactive joining and the experimental measurements of the shear strength of the stainless-steel joints indicates that the AuSn solder layers need to melt through their full 25  $\mu\text{m}$  thickness and be molten for a minimum period of time ( $\sim 0.5$  ms) to establish strong joints. Lastly, the numerical predictions and thermal

measurements demonstrate the very localized heating and very rapid cooling of reactive joining, which offers the ability to join temperature sensitive materials and components.

## ACKNOWLEDGMENTS

This work was supported by the National Science Foundation through Award No. DMI-0115238, and by Agilent Technologies Inc.

- <sup>1</sup>E. Ma, C. V. Thompson, L. A. Clevenger, and K. N. Tu, *Appl. Phys. Lett.* **57**, 1262 (1990).
- <sup>2</sup>L. A. Clevenger, C. V. Thompson, and K. N. Tu, *J. Appl. Phys.* **67**, 2894 (1990).
- <sup>3</sup>U. Anselmi-Tamburni and Z. A. Munir, *J. Appl. Phys.* **66**, 5039 (1989).
- <sup>4</sup>T. S. Dyer, Z. A. Munir, and V. Ruth, *Scr. Metall.* **30**, 1281 (1994).
- <sup>5</sup>T. W. Barbee Jr. and T. P. Weihs, U.S. Patent No. 5,538,795 (1996).
- <sup>6</sup>T. W. Barbee, T. P. Weihs, and M. Park, U.S. Patent No. 5,547,715 (1996).
- <sup>7</sup>A. E. Grigoryan, N. G. Elistratov, D. Y. Kovalev, A. G. Merzhanov, A. N. Nosyrev, A. S. Rogachev, V. I. Khvesyuk, and P. A. Tsygankov, *Dokl. Phys. Chem.* **381**, 368 (2001).
- <sup>8</sup>A. J. Gavens, D. V. Heerden, A. B. Mann, M. E. Reiss, and T. P. Weihs, *J. Appl. Phys.* **87**, 1255 (2000).
- <sup>9</sup>T. P. Weihs, *Handbook of Thin Film Process Technology* (Institute of Physics, UK, 1998).
- <sup>10</sup>J. L. McNaughton and C. T. Mortimer, *Differential Scanning Calorimetry* (Perkin-Elmer, Norwalk, CT).
- <sup>11</sup>T. P. Weihs, M. A. Wall, and T. W. B. Jr., *J. Mater. Res.* **11**, 1403 (1996).
- <sup>12</sup>C. Michaelsen, K. Barmak, and T. P. Weihs, *J. Phys. D* **30**, 3167–3186 (1997).
- <sup>13</sup>M. E. Reiss, C. M. Esber, D. V. Heerden, A. J. Gavens, M. E. Williams, and T. P. Weihs, *Mater. Sci. Eng., A* **261**, 217 (1999).
- <sup>14</sup>S. Jayaraman, O. M. Knio, A. B. Mann, and T. P. Weihs, *J. Appl. Phys.* **86**, 800 (1999).
- <sup>15</sup>E. Besnoin, S. Cerutti, O. M. Knio, and T. P. Weihs, *J. Appl. Phys.* **92**, 5474 (2002).